Polar Meteorol. Glaciol., **14**, 78–91, 2000

Heat and moisture budget and trajectory analysis of a warming event observed in June 1997 at Dome Fuji Station, Antarctica

Hiroaki Hatsushika and Koji Yamazaki

Graduate School of Environmental Earth Science, Hokkaido University, Kita-10 Nishi-5, Kita-ku, Sapporo 060-0810

Abstract: An abrupt warming event occurred during June 17 to June 19 at Dome Fuji Station (3810 m a.s.l.) in East Antarctica, in 1997. The surface air temperature increased from −70 °C to −30 °C in two days. The warming event was associated with the intrusion of an anticyclone onto the East Antarctic plateau. European Centre for Medium-Range Weather Forecasts (ECMWF) objective analysis data and Dome Fuji Station sonde data are used to investigate this event. Comparison between the sonde data and the ECMWF data shows reasonable agreement. The temperature increase exceeded 15 K at 400 hPa within 1.5 days, while the temperature at 150 hPa decreased 15 K. The heat and moisture budget analyses reveal that this tropospheric warming was caused by strong poleward advection of high potential temperature from lower latitudes, which overcame the cooling effect of the upward motion. On the other hand, stratospheric cooling was caused by the upward motion.

Five-day backward trajectory calculations from Dome Fuji Station are performed for June, 1997. Although almost all of the air parcels originated from inside of the polar vortex for the period before the warming, many parcels originated from mid-latitudes during and after the warming. This suggests that mixing of air between the polar and mid-latitude regions was enhanced during and after the warming event.

1. Introduction

During the meteorological observational period of the 38th Japanese Antarctic Research Expedition (JARE-38), the surface air temperature at Dome Fuji Station (39.70° E, 77.3° S, 3810 m above sea level, see Fig. 1 of Enomoto *et al.*, 1998 for the location) in Antarctica increased by about 40 K from 17th to 19th June in 1997 (Hirasawa *et al.*, 1999). The surface air temperature increased from −70°C to −30°C in two days. Similar warmings were observed at Relay Point in 1993 (Enomoto *et al.*, 1995) and at Dome Fuji Station in June, 1994 (Enomoto *et al.*, 1998, see Fig. 1 of their paper for the locations).

A drastic warming which was accompanied by invasion of an anticyclone and formation of cloud was seen in the summer of 1978 (Sinclair, 1981). Kikuchi *et al.* (1988) showed three-hourly variations of cloud amount and temperature at Mizuho Station and its Advanced Camp in East Antarctica in 1985. In that case, the cloud amount increased after the air temperature rose. According to Murata and Yamanouchi (1997), the monthly mean cloudiness over this area is about 1 in winter. During the warming in June 1997, the cloudiness suddenly increased to 10 (Hirasawa,

1999) and aerosol concentration also increased (Hayashi, 1999). During the warming, the sky was overcast with thick clouds. After the warming, the cloud became transparent and gradually stars could be seen.

Nakamura *et al.* (1997) showed that two major causes of blocking exist in the Northern Hemisphere. One is by quasi-stationary Rossby waves over the North Atlantic which is seen in Europe. He suggested that this mechanism also explains Southern Hemispheric blockings. The other is by transient eddies (*e.g.*, Blackmon *et al.*, 1986; Tsou and Smith, 1990; Chen and Juang, 1992) which is usually seen over the North Pacific. In the Southern Hemisphere, blocking over the South Pacific has been studied by Renwick (1998) and Renwick and Revell (1999). They showed the effect of quasi-stationary Rossby waves by using the quasi-geostrophic vorticity equation.

A 'blocking like' invasion of an anticyclone from mid-latitudes occurred at the beginning of the warming event in June 1997 (Hirasawa *et al.*, 2000, see their Fig. 1). They suggested that a strong blocking ridge was formed by a quasi-stationary Rossby wavetrain emanating from the subtropics. They mentioned that a strong poleward flow on the west side of the anticyclone pumped up heat and moisture from lower latitudes onto the East Antarctic plateau where Dome Fuji Station is located. However, quantitative analysis was not done in their study.

In this study, quantitative analysis of heat and moisture budget for this warming event is performed using the ECMWF objective analysis data, in order to clarify the cause of the warming. In addition, the air mass exchange between the inland Antarctica (Dome Fuji Station) and lower latitudes is investigated by backward trajectory analysis.

2. Data and analysis method

2.1. Data

The data sets used in this study are the twice-daily ECMWF/TOGA objective analysis data (hereafter referred to as ECMWF data) and Väisalä GPS Sonde (80-15G) data at Dome Fuji Station (hereafter referred to as sonde data). The sonde data were acquired irregularly (from four times a day to one in 5 days) during the period from February 15, 1997 to January 7, 1998. The ECMWF data for the same period are used.

In the vertical, the ECMWF data set has 15 pressure levels (1000, 925, 850, 700, 500, 400, 300, 250, 200, 150, 100, 70, 50, 30, and 10 hPa) and the horizontal resolution is $2.5^\circ \times 2.5^\circ$ in longitude and latitude. Parameters used in this study are geopotential height (z), temperature (T), zonal wind (U), meridional wind (V), relative humidity (RH), surface pressure (P_s), temperature at 2 m above the ground ($T_{2\,m}$), zonal wind at 10 m above the ground ($U_{10\,m}$), meridional wind at 10 m above the ground ($V_{10\,m}$) for the ECMWF data and geopotential height (z), temperature (T), and pressure (P) for the sonde data.

2.2. Analysis method for heat and moisture budgets

For the analysis of heat and moisture budgets, we use the apparent heat source and apparent moisture sink by following Yanai *et al.* (1973). The *dry static energy* is defined as

$$s \equiv c_p T + gz, \tag{1}$$

where s is the sum of enthalpy and potential energy. s is conserved in an adiabatic process. Then s/c_p is the temperature when an air parcel is moved dry-adiabatically to zero geopotential height (hereafter referred to as 'quasi-potential temperature'). Combined with the continuity equation, the material derivative of the dry static energy becomes

$$\frac{ds}{dt} = \frac{\partial s}{\partial t} + \nabla s v_h + \frac{\partial s\omega}{\partial p}. \tag{2}$$

The *apparent heat source*, Q_1 is defined as

$$Q_1 \equiv \frac{\partial \bar{s}}{\partial t} + \overline{\nabla \bar{s} \bar{v}_h} + \frac{\partial \bar{s}\bar{\omega}}{\partial p} \tag{3}$$

$$= Q_R + L(c-e) - \left(\overline{\nabla s' v_h'} + \frac{\overline{\partial s' \omega'}}{\partial p} \right), \tag{4}$$

where v_h and ω are horizontal velocity and vertical p-velocity, Q_R is heating rate due to radiation, and L, c and e are latent heat of condensation, the rate of condensation and the rate of re-evaporation, respectively. The overbar denotes the areal average and the prime denotes the deviation from the areal average. Q_1 is calculated from the grid-scale values from eq. (3).

The *apparent moisture sink*, is defined in a similar fashion, as

$$Q_2 \equiv -L\left(\frac{\partial \bar{q}}{\partial t} + \overline{\nabla \bar{q} \bar{v}_h} + \frac{\partial \bar{q}\bar{\omega}}{\partial p} \right) \tag{5}$$

$$= L(c-e) + L\left(\overline{\nabla q' v_h'} + \frac{\overline{\partial q' \omega'}}{\partial p} \right), \tag{6}$$

where q is the mixing ratio of water vapor. The cross-prime terms represent subgrid-scale fluxes, mainly due to convection, which are large in the tropics but small in the polar regions.

To estimate Q_2, we need to calculate the mixing ratio of water vapor from relative humidity, temperature and pressure. Because the Tetens formula is used in the ECMWF to calculate the RH data, we also use the Tetens formula for calculation of the saturation mixing ratio of water vapor as follows.

First, we calculate the saturation water vapor pressure E_s for both liquid water and ice by

$$E_s = 6.11 \times 10^{\frac{a(T-T_0)}{b+(T-T_0)}}, \tag{7}$$

where $T_0 = 273.15$ K. Constant factors a and b are given as

$$(a, b) = \begin{cases} (9.5, 265.5), & \text{on ice} \\ (7.5, 237.3). & \text{on water} \end{cases}$$

The saturation mixing ratio q_s is expressed by

$$q_s(\text{water or ice}) = 0.622 \times \left(\frac{E_s}{P - E_s} \right), \tag{8}$$

where P is pressure. In the ECMWF model, q_s is multiplied by a factor α to interpolate the ice and water condition as

$$\alpha=\begin{cases} 0, & \text{for } T\leq T_{\text{ice}} \\ \left(\dfrac{T-T_{\text{ice}}}{T_0-T_{\text{ice}}}\right)^2, & \text{for } T_{\text{ice}}\leq T\leq T_0 \\ 1, & \text{for } T\geq T_0 \end{cases}$$

where $T_{\text{ice}}=T_0-23\,\text{K}$.

Then the mixing ratio of water vapor q is calculated as

$$q=(\alpha\times q_s(\text{water})+(1-\alpha)\times q_s(\text{ice}))\times RH\times 0.01. \quad (9)$$

2.3. *Trajectory analysis*

To explore the origin of the air parcels over Dome Fuji Station, a trajectory calculation is done. Trajectories of air parcels which are initially placed above and around Dome Fuji Station are calculated backward in time for 5 days. The 3-dimensional trajectories are calculated by using the ECMWF horizontal wind components u and v, and ω. The ω is obtained by integrating the mass continuity equation downward (Yamazaki, 1992). The upper boundary condition $\omega=0$ is applied at 1 hPa.

The time step for the advection calculation is 20 min, and the 3-dimensional winds are linearly interpolated in time from the original 12-hourly data. Spatially, we used linear interpolation in the horizontal and cubic spline interpolation in the vertical.

3. Results

3.1. *Overview of the warming event*

Figure 1 shows the seasonal variations of the 400 hPa and 150 hPa geopotential height and temperature fields at Dome Fuji Station during JARE-38 (from February

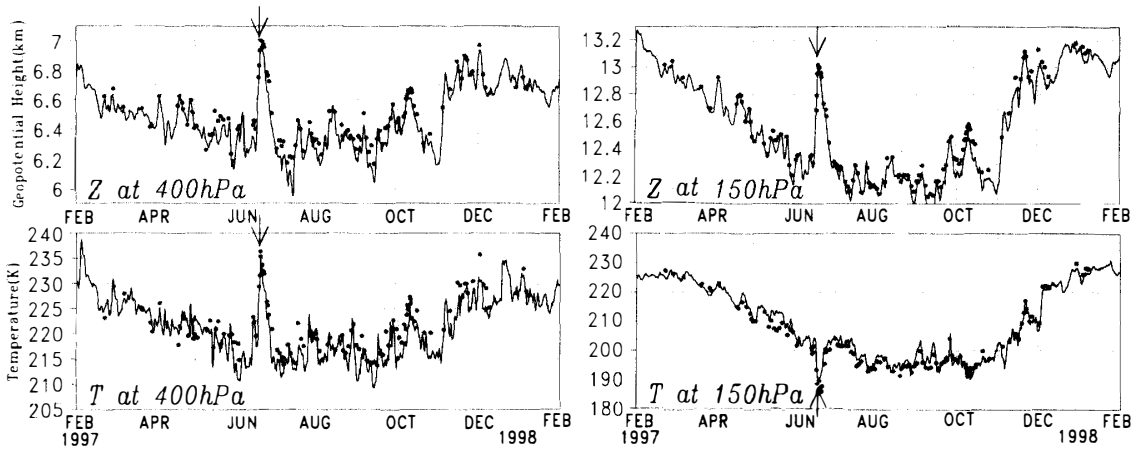

Fig. 1. Seasonal change in the geopotential height (upper) and the air temperature (lower) at 400 hPa (left) and 150 hPa (right) at Dome Fuji Station, based on sonde observations from February 1997 to January 1998. The solid lines denote the interpolated ECMWF data and the dots denote the Dome Fuji Station sonde data.

15th in 1997 to January 7th in 1998). The sonde data are shown by dots and the ECMWF data are shown by lines. For the ECMWF data, values are linearly interpolated to the location of Dome Fuji Station from values of the surrounding grid points. In general, the ECMWF data agree well with the sonde data. In particular, the warming event in June, which is denoted by an arrow, is well captured by the ECMWF data, hence the ECMWF data can be used for the analysis of the warming event.

It is obvious that the temperature is colder (warmer) and the geopotential height is lower (higher) in winter (summer), and warming in spring is more rapid than cooling in autumn, as shown by many analyses of polar sonde and satellite data (*e.g.*, Van Loon, 1967; Nakamura and Oort, 1988; Kikuchi *et al.*, 1988). The most interesting features found in Fig. 1 are the warming event at 400 hPa and the cooling event at 150 hPa, which are especially prominent on June 18. Dramatic surface warming occurred at the same time. A similar event took place from June 13 to 14, 1994 (Enomoto *et al.*, 1998). The temperature at 400 hPa on June 18 became as high as the hottest summer value, and the temperature at 150 hPa became the coldest of the year. The geopotential height also increased during the warming event at both levels.

Figure 2 shows the potential temperature variations calculated using the ECMWF data on isobaric surfaces at Dome Fuji Station during June, 1997. The potential temperature abruptly rose below 250 hPa and dropped above 250 hPa from June 17 to 18. The potential temperature at 200 hPa began to increase from June 18. Initially, the warming was confined to the troposphere, while cooling occurred in the stratosphere. Temperatures at lower levels increased while temperatures at upper levels decreased. Therefore, stratification becomes less stable, especially around 200 hPa to

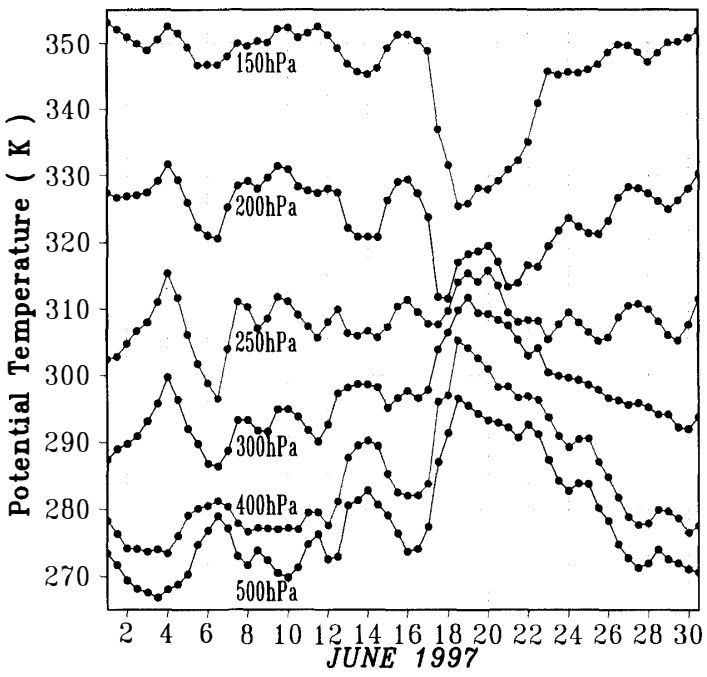

Fig. 2. Potential temperature variation calculated from the ECMWF data during June 1997. Six levels (150, 200, 250, 300, 400, 500 hPa) are shown.

300 hPa. To confirm this, we calculated the gradient Richardson number (Ri), which represents atmospheric stability, at the beginning of this warming event. From the ECMWF data, Ri suddenly decreased to less than 1 in the layers between 250 hPa and 300 hPa and between 200 hPa and 250 hPa at the nearest grid of Dome Fuji Station. From the sonde data, Ri became smaller than 1/4 in the layer between 250 hPa and 300 hPa. Therefore, the stratification became less stable, especially around 200 hPa to 300 hPa.

The increase of the surface pressure and the tropospheric warming produced a large geopotential height increase in the troposphere. In spite of the cooling in the stratosphere which reduced the thickness there, the geopotential height in the lower stratosphere increased. The anomaly decreased with altitude and became unnoticeable above 10 hPa.

After the peak of the event, temperatures and geopotential height slowly returned to the previous values for about ten days with gradual restoration of the polar vortex.

3.2. Heat and moisture budgets

The cooled layer was located between 100 hPa and 250 hPa, and was almost in the stratosphere. The warmed layer was located below 250 hPa. Although large warming was also observed near the ground, we do not include the lowest layers in this study, because of the coarse vertical resolution of the ECMWF data. As the surface pressure at Dome Fuji Station is around 600 hPa, between 300 hPa and 500 hPa is chosen as a representative layer for the tropospheric warming. Similarly between 100 hPa and 200 is chosen for the layer of stratospheric cooling. The heat and moisture budgets at these two levels are shown to clarify the causes of warming and cooling.

Figures 3a and b show the heating rates between 300 hPa and 500 hPa. The line with open circles (a-1) in Fig. 3a shows the heating rate due to horizontal advection, $-v_h \nabla s/c_p$, while the line with closed circles (a-2) shows that due to vertical advection, $-\omega(\partial s/\partial p)/c_p$. The sum of the two is shown by the solid line (a-3). Horizontal advection has large positive values during the warming event, while vertical advection has negative values during the same period. The sum of the two shows positive values. This shows that, during the warming event, warm horizontal advection significantly offset the cooling effect due to vertical motion, thus causing net warming.

After the warming, the heating rate due to horizontal advection became negative, while that due to vertical advection became positive. Thereafter, the atmosphere gradually cooled by adiabatic processes.

In Fig. 3b, the line with open squares (b-1), $(\partial s/\partial t)/c_p$ shows the local warming rate over Dome Fuji Station. The quasi-potential temperature change exceeded 12 K/day during the warming. The solid line (b-3) in Fig. 3b is the same as in Fig. 3a and shows the adiabatic heating rate. The difference between the local warming rate and the adiabtic heating rate, which is the *apparent heat source* Q_1/c_p, is given by the line with closed squares (b-2). Q_1 shows positive values during the warming event and negative values before and after the event. Physically, Q_1 consists of radiative heating Q_R, grid-scale condensation heating, grid-scale evaporative cooling and subgrid-scale heatings. The apparent moisture sink Q_2, which is approximately equal to $Q_1 - Q_R$ in the absence of subgrid-scale heating, divided by c_p, is shown in Fig. 3c. Q_2 was quite small

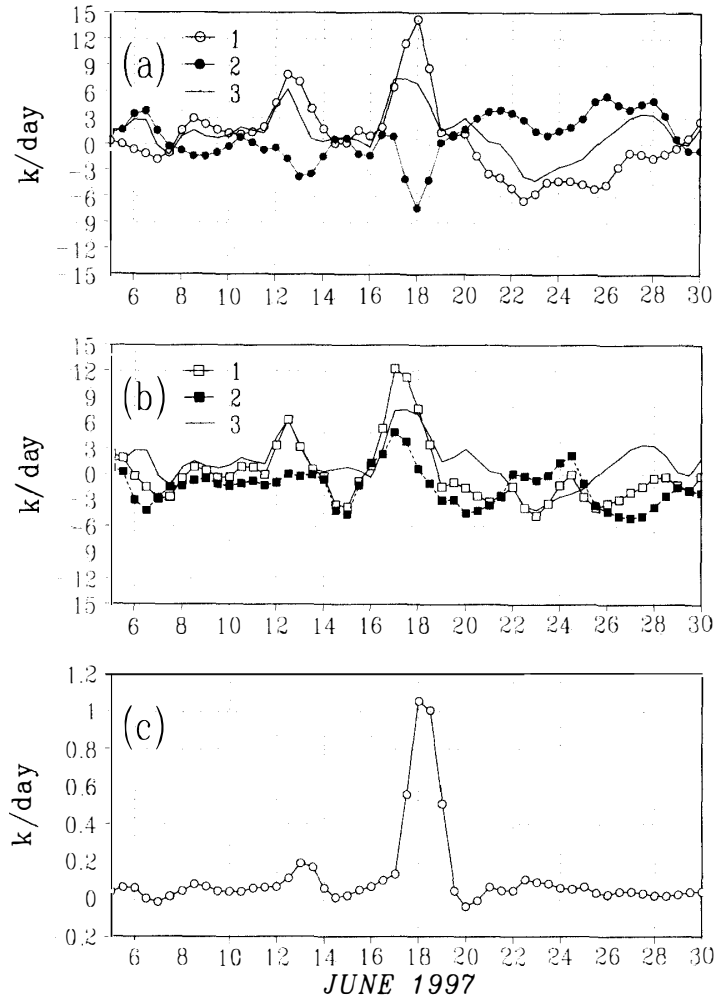

Fig. 3. Each component of the heating rate between 300 hPa and 500 hPa during the period from 5th to 30th June, 1997. (a) a-1, a-2, and a-3 correspond to the horizontal advection term, vertical advection term, and total advection term, respectively. (b) b-1, b-2, and b-3 correspond to the local time derivative, the total advection term, and the apparent heat source divided by c_p, respectively. (c) apparent moisture sink divided by c_p. The unit of the ordinate is K/day and values are averaged over 30°E–50°E, 75°S–80°S. Variations with periods shorter than one day are filtered out.

except during the warming period. The sharp peak in Q_2/c_p during the warming event was over 1 K/day, consistent with the observed thick cloud over Dome Fuji Station (Hirasawa *et al.*, 2000). The condensational heating contributed to the warming to some extent, though the heating was not enough to explain all of Q_1. Radiation might have played a role in compensating for the net deviation of Q_1.

Moisture transport onto the Antarctic plateau occurs sporadically in association with intrusions of anticyclones. During winter, moisture transport into inland Antarctica is usually suppressed because of the strong polar vortex. Intrusion of anticyclones, which occurs sporadically, greatly enhances the moisture transport. Therefore, warming events played a major role in the wintertime moisture budget over Antarctica.

Figure 4 is the same as Fig. 3 but the layer is between 100 hPa and 200 hPa. In

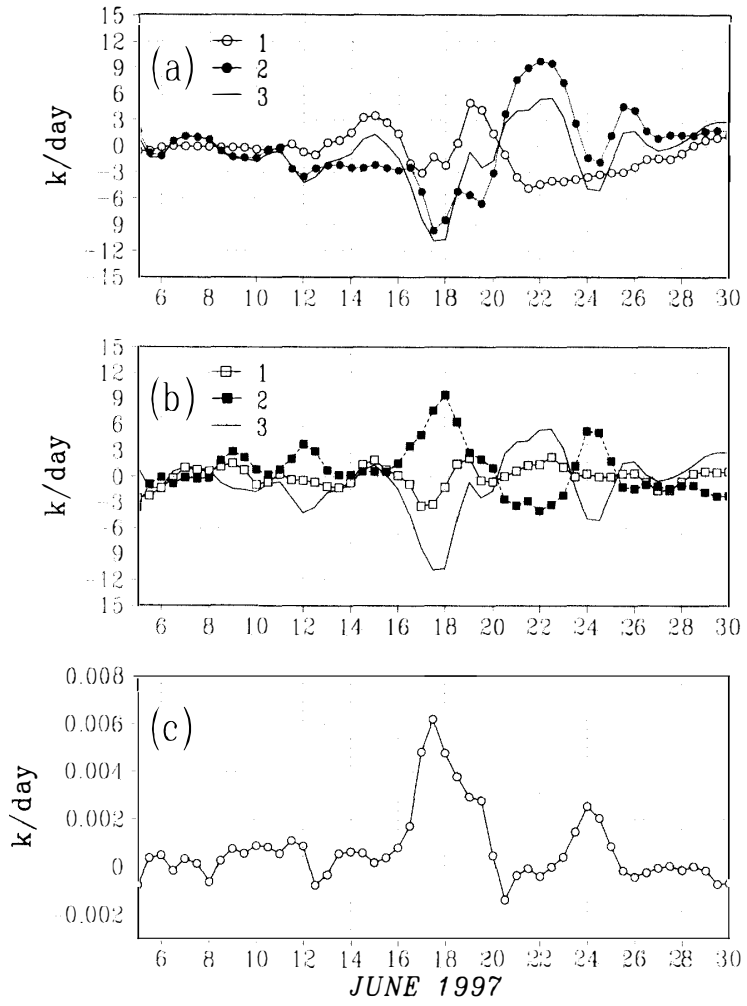

Fig. 4. Same as Fig. 3 but the layer is between 100 hPa and 200 hPa.

Fig. 4a, there was large adiabatic cooling during the warming event in Fig. 3. At this level, however, vertical advection was the dominant source of cooling, while the horizontal component acted only as a small contributor to the cooling. Throughout the layer from the surface to the lower stratosphere, the upward motion was dominant. Warm advection more than compensated for the cooling effect in the troposphere due to upward motion, while in the lower stratosphere, the contribution from horizontal advection was small while the cooling effect due to upward motion was dominant. In the Northern Hemisphere, a blocking high frequently causes tropospheric warming mainly due to downward motion. In this respect, the present Antarctic warming has a different mechanism from the usual NH warming associated with a blocking high.

After the cooling, the vertical advective heating started to show large positive values. The layer between 100 hPa and 200 hPa gradually warmed by adiabatic processes, which was not the case between 300 hPa to 500 hPa (Fig. 3). From Fig. 4c, it can be seen that Q_2 contributed very little to the total heating rate between 100 hPa and 200 hPa.

Figure 5 shows the mean (v, ω) maps from 30°E to 50°E at 12 UTC, June 17 and

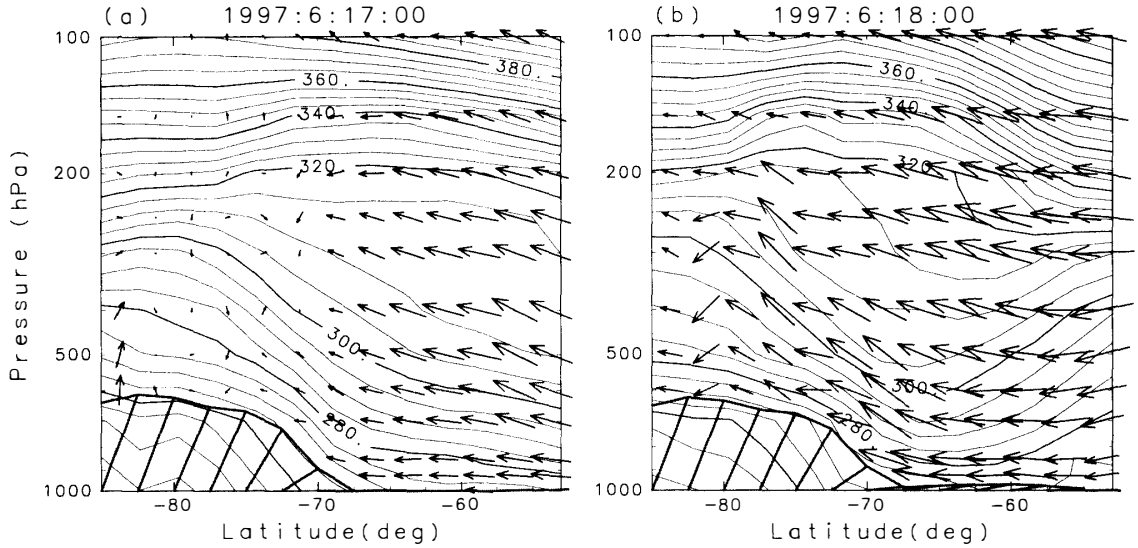

Fig. 5. The latitude-height cross sections of mean wind (meridional wind and vertical velocity, 30°E-50°E) and potential temperature at 00 UTC June 17 (a) and 00 UTC June 18 (b). The section covers 85°S-53°S and 1000 hPa-100 hPa. Thick lines show the ground surface and arrows show the 4-hour displacements. Winds at 600 hPa are interpolated by a cubic spline function.

12 UTC, June 18, which are the beginning of the warming event and the warming peak, respectively. Although the contribution of zonal wind is not considered, it is easy to see that the northerly wind is orographically lifted at the edge of the continent. This effect can be seen into the lower stratosphere. This is the reason why the structure of blocking over East Antarctica is generally different from the ordinary case. This strong northern wind, which is driven by invasion of the anticyclone, climbs the continental surface and produces the warm and moist condition in inland Antarctica.

There usually exists a strong latitudinal gradient of potential temperature in the troposphere. Therefore, the northern wind produces strong warm advection. We suggest that the warming occurred by strong horizontal advection of air with high potential temperature in spite of adiabatic cooling by upward motion in the lower layer. Since the atmosphere is usually rich in moisture in the lower level and over the ocean, the northern wind with upward motion produced moist air advection, causing increase in cloudiness and warming over Dome Fuji Station. In the upper layer, cooling by upward motion dominated (see also Fig. 4). A comparison between Fig. 5a and b reveals that the tropopause level was lifted up due to the upward motion. Lifting of the tropopause was also observed by Sinclair (1981).

Fig. 6 (opposite). Trajectories of 825 air parcels which are advected backward from Dome Fuji Station by three dimensional wind for five days. In these maps, horizontal trajectories are shown on the left hand side and the meridional locations of parcels 5 days ago on the right hand side. (a) from May 31 to June 5. (b) from June 14–19. (c) from June 19–24. Parcels which are advected to the upper layer of Dome Fuji Station are drawn in pale lines and dots, while those to the lower layer are in dark lines and dots.

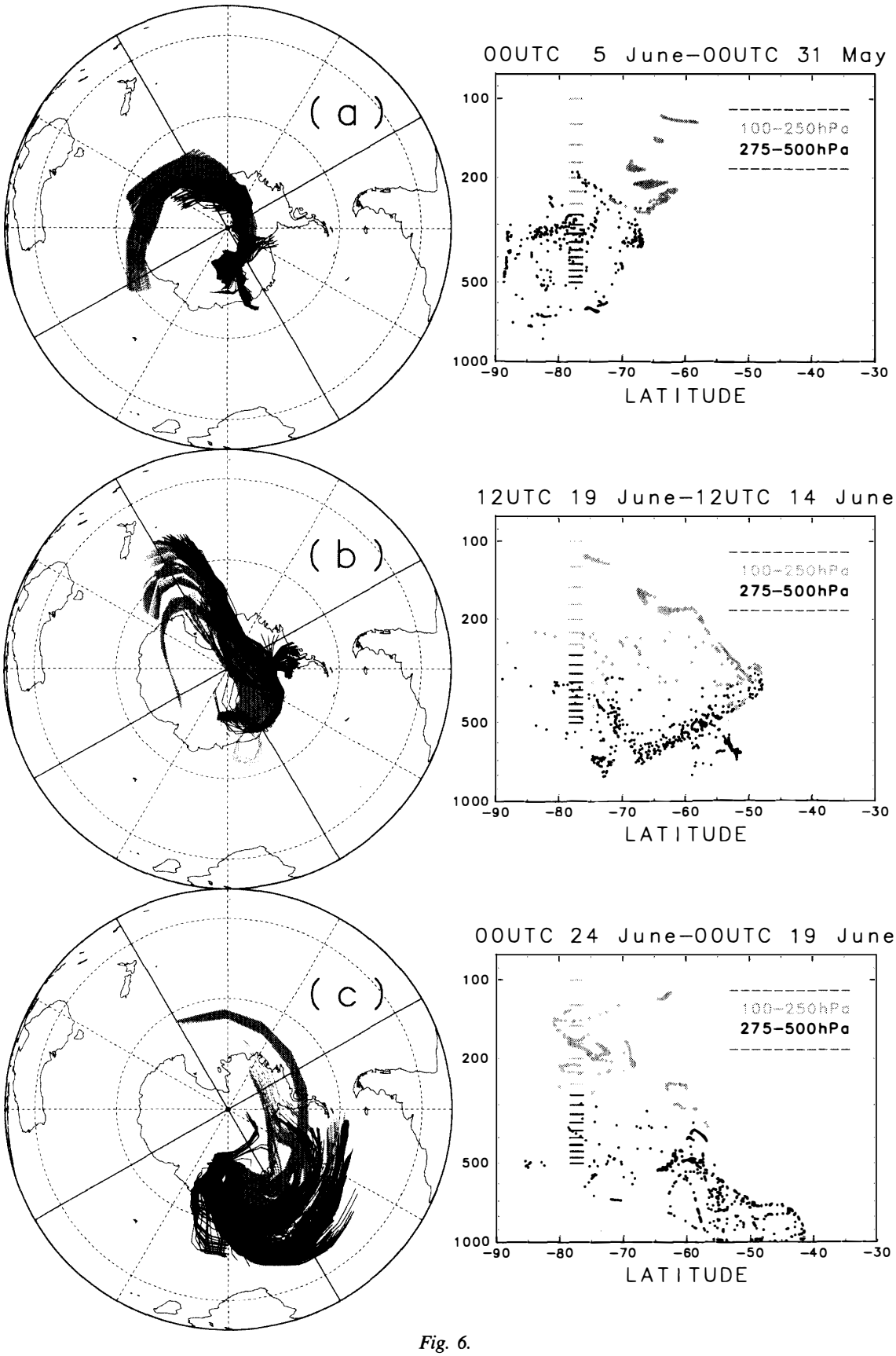
(a)
00UTC 5 June–00UTC 31 May
100–250hPa
275–500hPa
100
200
500
1000
–90 –80 –70 –60 –50 –40 –30
LATITUDE
(b)
12UTC 19 June–12UTC 14 June
100–250hPa
275–500hPa
100
200
500
1000
–90 –80 –70 –60 –50 –40 –30
LATITUDE
(c)
00UTC 24 June–00UTC 19 June
100–250hPa
275–500hPa
100
200
500
1000
–90 –80 –70 –60 –50 –40 –30
LATITUDE

Fig. 6.

3.3. *Trajectory analysis*

The characteristics of the air parcel transport during June are studied by trajectory calculations. Initially, we put parcels within the small area over Dome Fuji Station. Its size is 2° in the zonal direction and 1° in the meridional. In the vertical, we put parcels at every 25 hPa from 500 hPa to 100 hPa. Parcels are advected for 5 days backward in time. Trajectories for typical cases are shown on the left-hand side of Fig. 6. In this study, 5 days is chosen as the representative lifetime of mesoscale disturbances. The right-hand side of Fig. 6 shows the original (5 days before) positions of air parcels for each case. The period of map (a) is May 31–June 5, which represents 'before the warming event'. Air parcels remained in the core of the winter vortex. Map (b) is for the period June 14–19, which represents 'during the warming event' and map (c) for June 19–24, 'after the warming event'. It is obvious that parcels in maps (b) and (c) came from lower latitudes than (a). The right-hand side of map (b) shows the air parcels came from the middle troposphere in mid-latitude. The trajectory of map (b) shows that air parcels which were initially located south of New Zealand were advected along the edge of the Antarctic plateau, lifted by the northerly wind on June 17, and brought to Dome Fuji Station by westerly flow of the invading anticyclone. On the other hand, the wave train which caused warming emanated from the anticyclonic anomalies in the subtropical South Atlantic (see Fig. 2 of Hirasawa *et al.*, 2000). This shows a typical case in which the sources of material advection and wave propagation are different.

At and after the warming event, the air parcels over Dome Fuji Station appeared to originate from lower latitudes compared with the pre-warming period. To confirm this, we calculated the mean latitudinal positions of air parcels 5 days prior to arriving at Dome Fuji Station (Fig. 7). In Fig. 7, the stars denote the upper layer and closed

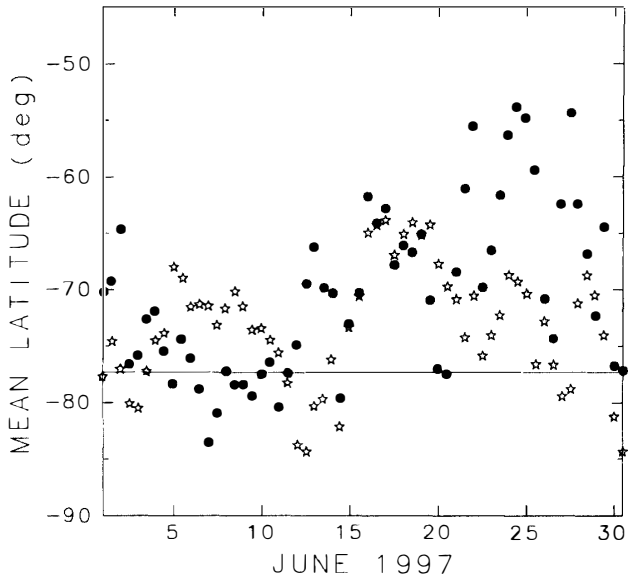

Fig. 7. The mean initial latitude of air parcels which are advected backward for 5 days. Conditions are the same as in Fig. 6. The parcels advected to the upper layer are drawn with stars and those to the lower layer with closed circles. The line indicates the location of Dome Fuji Station (77.3°S).

circles denote the lower layer. In early June, air parcels in both layers originated from high latitude, 5 days before. But in mid-June, when the anticyclone approached and the cyclonic vortex core began to collapse, air parcels were transported from lower latitudes.

This transport situation continued for a while. The situation gradually returned to the pre-warming condition for about 10 days in the lower layer and about 5 days in the upper layer.

4. Summary and discussion

In this study the mechanism of the tropospheric warming which occurred in June 1997 over Dome Fuji Station is examined by using the ECMWF data.

From the 17th to 19th of June 1997, an intense warming of about 40 K at the ground and about 15 K in the middle troposphere was observed by sonde observation at Dome Fuji Station, Antarctica. At the same time, the lower stratospheric temperature decreased abruptly. This tropospheric warming event was associated with the intrusion of an anticyclone onto the East Antarctic plateau, and the geopotential height increased up to the lower stratosphere. After the event, their anomalies slowly decreased.

Accompanying the intrusion of the anticyclone from mid-latitude, a strong northern wind at the edge of Antarctica was topographically lifted, inducing a strong upward velocity. Though this upward motion decreased the temperature by adiabatic cooling, the horizontal advection of higher potential temperature from lower latitudes overcame the cooling. It is clear that the net heat budget is positive in the lower layer. Although most of the observed warming in the lower layer can be explained by the adiabatic process, other processes contributed to the warming, because Q_1 is large positive during the warming event. Q_1 can be explained partly by condensation heating, Q_2. The imbalance of the budget may be compensated for by radiational heating.

In the upper layer, it is found that the sudden decrease of temperature was mainly caused by upward advection. However, positive Q_1 is also calculated during the warming event. Q_2 was too small to compensate for Q_1. Part of the gap may be filled with radiational heating due to cloud. A simple calculation of radiation with intruded cirrus clouds gives a 1–2 K/day heating rate and could make up for the gap in the heat budget. We should calculate this wintertime cloud effect more precisely.

The mixing of the polar air and the mid-latitude air is usually weak during the austral winter. Trajectory analysis of the air parcels from the Dome Fuji Station during June is performed by using the ECMWF data. Almost all of the air parcels originated from inside of the polar vortex during the period before the warming. During and after the warming, however, many air parcels originated from lower latitudes. The invasion of the anticyclone weakened the strong wintertime vortex core and enhanced the mass exchange between Antarctica and mid-latitudes. This enhanced mixing situation clearly continued until the polar core was restored. It lasted longer in the lower layer. During the warming period, many parcels of both layers were advected from the middle troposphere in mid-latitude. After the warming period, many parcels in the lower layer were advected from the mid-latitude lower troposphere.

From the observed correlational relationship between the meridional wind and the potential temperature fields (Fig. 5), it can be seen that advection of air from mid-latitudes during a warming event can cause the lower layer (from 300 hPa to 500 hPa) to warm, and upward motion due to orographic lifting can cause the upper layer (from 100 hPa to 200 hPa) to cool over Dome Fuji Station. After the warming event, air in the lower layer over Dome Fuji Station was advected from the mid-latitude lower troposphere where the potential temperatures were observed to be lower than those in the lower layer over Dome Fuji Station. This resulted in cooling of the lower layer at Dome Fuji Station. This interpretation is consistent with the heat budget analysis results. We studied one warming event which occurred in June 1997 over Antarctica. Similar events have been observed in other years. Further studies are needed to see if the results of the present study are commonly applicable to other warming cases.

Acknowledgments

We thank N. Hirasawa of the National Institute of Polar Research for providing us with sonde observation data over Dome Fuji Station, and his many useful discussions and comments.

References

Blackmon, M.L., Mullen, S.L. and Bates, G.T. (1986): The climatology of blocking events in a perpetual January simulation of a spectral general circulation model. J. Atmos. Sci., **43**, 1379–1405.

Chen, W.Y. and Juang, H.-M.H. (1992): Effects of transient eddies on blocking flows: General circulation model experiments. Mon. Weather Rev., **120**, 787–801.

Enomoto, H., Warashina, H., Motoyama, H., Takahashi, S. and Koike, J. (1995): Data-logging automatic weather station along the traverse route from Syowa Station to Dome Fuji. Proc. NIPR Symp. Polar Meteorol. Graciol., **9**, 66–75.

Enomoto, H., Motoyama, H., Shiraiwa, T., Saito, T., Kameda, T., Furukawa, T., Takahashi, S., Kodama, Y. and Watanabe, O. (1998): Winter warming over Dome Fuji, East Antarctica and semiannual oscillation in the atmospheric circulation. J. Geophys. Res., **103**, 23103–23111.

Hayashi, M. (1999): Observations of aerosol and trace constituents at Dome Fuji Station in Antarctica. Tenki, **46**, 153–156 (in Japanese).

Hirasawa, N. (1999): Summary of the atmospheric observation with meteorological sonde and of radiation and cloud at Dome Fuji Station in Antarctica and preliminary results. Tenki, **46**, 147–152 (in Japanese).

Hirasawa, N., Hayashi, M., Kanemoto, S. and Yamanouchi, T. (1999): Aerological sounding data at Dome Fuji Station in 1997. Data of Project on Atmospheric Circulation and Material Cycle in the Antarctic, Part 1. JARE Data Rep., **238** (Meteorology 32), 183 p.

Hirasawa, N., Nakamura, H. and Yamanouchi, T. (2000): Abrupt changes in meteorological conditions observed at an inland Antarctic station in association with wintertime blocking. Geophys. Res. Lett., **27**, 1911–1914.

Kikuchi, T., Ageta, Y., Okuhira, F. and Shimamoto, T. (1988): Climate and weather at the Advanced Camp in East Queen Maud Land, Antarctica. Bull. Glaciol. Res., **6**, 17–25.

Murata, A. and Yamanouchi, T. (1997): Distribution characteristics of clouds over East Antarctica in 1987 obtained from AVHRR. J. Meteorol. Soc. Jpn., **75**, 81–93.

Nakamura, N. and Oort, A.H. (1988): Atmospheric heat budgets of the polar regions. J. Geophys. Res., **93**, 9510–9524.

Nakamura, H., Nakamura, M. and Anderson, J.L. (1997): The role of high- and low-frequency dynamics in

blocking formation. Mon. Weather Rev., **125**, 2074–2093.
Renwick, J.A. (1998): ENSO-related variability in the frequency of South Pacific blocking. Mon. Weather Rev., **126**, 3117–3123.
Renwick, J.A. and Revell, M.J. (1999): Blocking over the South Pacific and Rossby wave propagation. Mon. Weather Rev., **127**, 2233–2247.
Sinclair, M.R. (1981): Record-high temperatures in the Antarctic–A synoptic case study. Mon. Weather Rev., **109**, 2234–2242.
Tsou, C.-H. and Smith, P.J. (1990): The role of synoptic/planetary-scale interactions during the development of a blocking anticyclone. Tellus, **42A**, 174–193.
Van Loon, H. (1967): The half-yearly oscillations in middle and high southern latitudes and the coreless winter. J. Atmos. Sci., **24**, 472–486.
Yamazaki, K. (1992): The statistical analysis of long-term trajectory calculation based on the observed data. J. Meteorol. Soc. Jpn., **70**, 1167–1173.
Yanai, M., Esbensen, S. and Chu, J.-H. (1973): Determination of bulk properties of tropical cloud clusters from large-scale heat and moisture budgets. J. Atoms. Sci., **30**, 611–627.

(Received March 6, 2000; Revised manuscript accepted July 18, 2000)